Seismic behaviour of multi-storey gravity-controlled rocking braced-frame buildings including floor vertical response

Paul Mottier[1], Robert Tremblay[2], and Colin Rogers[3]

[1]Graduate Researcher, [2]Professor, Department of Civil, Geological and Mining Engineering, Polytechnique Montreal, Montreal, Canada

[3]Professor, Department of Civil Engineering and Applied Mechanics, McGill University, Montreal, Canada

Abstract

Gravity-controlled rocking braced frames (G-CBRFs) are cost-effective low-damage self-centring lateral force resisting systems that allow the reduction of the seismic force demands in structures subjected to earthquakes, while relying only on the gravity loads they carry to ensure self-centring. Due to column uplift, significant masses are mobilized, thus activating vertical fundamental modes of vibration that affect the overall seismic behaviour of the structures. This article presents an examination of the seismic response of G-CBRF structures, including the response of the roof and floor framing systems. Twenty-two buildings were designed for this study, with various combinations of building heights (2-, 4-, and 8-storeys), building locations (eastern and western Canada), site classes (soil C and E), and location of the braced frame within the building (interior or exterior column lines). For each design, two framing configurations were studied, with secondary beams parallel or perpendicular to the braced frames. Non-linear response history analyses were performed using representative ground motions selected and scaled according to the National Building Code of Canada requirements. Effects of the vertical component of the ground motions and energy dissipated through friction in beam-to-column connections were also of focus. Incremental dynamic analyses were performed to generate fragility curves for collapse due to overturning of the studied structures. The results show that peak drifts can be accurately predicted. Peak axial loads in frame members are increased due to the vertical inertia forces induced upon rocking. The fragility curves show that acceptable margins against collapse by overturning is achieved for G-CRBFs.

Keywords: Steel braced frames; Rocking; Coupled braced frames; Collapse Assessment; Fragility curves

1. Introduction

Controlled rocking braced steel frame buildings have been increasingly studied in recent years, for they exhibit excellent performance in terms of seismic resiliency and efficient seismic behaviour [1–3]. Their use as a seismic force resisting system allows for the reduction of axial loads in the braced frame members, while maintaining acceptable drifts [4]. Furthermore, braced frame members are expected to remain elastic under severe earthquakes so that structural damage is avoided and post-earthquake downtime periods are minimized, thereby reducing the building cost over its life cycle. To help control building drifts, energy dissipative (ED) devices can be installed at the base of the columns [1,3] or along their heights [2,4]. Rocking braced frames can be decoupled from the gravity framing system. In that case, self-centring capacity is generally achieved by means of vertical post-tensioned (PT) strands linking the top of the rocking braced frame to the foundation to form PT-CRBFs. Alternatively, CRBFs can be part of the gravity framing system so that self-centring capacity can be provided by the gravity loads supported by the frame [5]. CRBFs of that configuration are referred to as gravity-controlled rocking braced frames (G-CRBFs). Past numerical and experimental studies have demonstrated the efficiency of G-CRBFs for controlling seismic induced member forces and drifts, both for the seismic retrofit of existing structures and new building applications [1, 5-8]. In G-CRBFs, floor and roof beams framing into the braced frames are uplifted when rocking occurs during an earthquake. This introduces additional vertical modes of vibration that are excited by column uplifting from and impacting against foundations, resulting in increased member forces in the braced frame and adjacent floor and roof structures [8]. The contribution of these vertical vibration modes to the frame member forces was investigated in [9], and the results showed the effects from vertical response generally diminished as the building height was increased. This study was, however, performed on a planar (2D) frame model in which roof and floor masses were lumped at the beam-to-column nodes of the rocking frames, hence ignoring dynamic response of the roof and floor beams.

This article presents a numerical study that was performed to verify if satisfactory seismic response could be obtained for G-CRBF buildings up to 8-storeys located in both eastern and western seismic regions of Canada. The purpose of this study was also to assess the influence of the dynamic behaviour of the roof and floor gravity framing systems on the seismic induced braced frame forces, and verify if gravity loads were sufficient to provide safety against collapse by overturning. Complementary analyses were performed to evaluate the effects of the vertical component of ground motions on the G-CRBF member forces, and to examine the possible beneficial effect of the inherent friction in bolted beam-to-column connections on frame drifts and member forces. To achieve these objectives, a group of 22 different prototype buildings was examined. Three different building heights (2-, 4-, and 8-storeys) as well as different building locations (Vancouver, BC in western Canada, and Montreal, QC, in eastern Canada), site classes (C and E) and braced frame locations (along exterior or interior column lines) were studied. Friction based ED devices were implemented at the base of the rocking braced frame columns to achieve the required minimum overturning moment capacity and control drifts. The rocking frames were designed using the force-based approach of the 2015 National Building Code of Canada [10], with a global force modification factor varying from 3.5 to 8.0 depending upon the building location, gravity load on the frame, and ED resistance. Nonlinear response history analysis of the structures was performed using Opensees [11] under site-compatible ground motions. Three-dimensional analysis models were used to evaluate explicitly include the vertical response of the roof and floor beams framing into G-RCBFs. Fragility curves developed for PT-CRBFs in previous studies [12,13] have shown that the system can exhibit satisfactory seismic performance when designed with R factors in the order of 8. For G-CRBFs, in absence of PT strands, collapse by overturning could represent a concern in design and fragility curves were therefore generated for the frames studied to evaluate the margins they offered against this ultimate limit state.

2. Design of the Prototype Buildings

This study was performed on 22 G-CRBF prototype buildings having 2, 4 and 8 storeys located in two cities in Canada: Montreal, Quebec (M), and Vancouver, British Columbia. Montreal is situated in a moderately-active seismic zone of eastern North America characterized by earthquakes rich in high frequencies. The seismic hazard is higher at Vancouver, being contributed by crustal and large subduction earthquakes with longer dominant periods. Two site classes were also considered in the study: site class C (very dense soil and soft rock) and site class E (soft soil), as well as two braced frame locations in the buildings: along exterior column lines (E) or interior column lines (I). In G-CRBFs, overturning moment resistance is obtained from column gravity loads as well as ED resistance at the column base. The location and site class affect the design seismic overturning moment and changing the location of the frame in the structure affects the available column gravity load. For each building, the ED resistance was adjusted to achieve the required overturning moment resistance. The properties of the 22 buildings are presented in Table

1. The building ID is composed of the city tag (M or V), the site class tag (C or E), the number of storeys, the location of the frame (E or I), and the effective force modification factor, R_{eff}, as defined later. Furthermore, for each of the 22 buildings, the response was studied along both orthogonal directions to examine the effects of the direction of the secondary beams with respect to the G-CRBFs, being either perpendicular (*Perp*) or parallel (*Para*).

The plan view of the studied buildings is given in Figure 1 a. All braced frame arrangements studied are shown in the figure: buildings with rocking braced frames along exterior or interior column lines, and buildings with one rocking braced frame per column line ($N_f = 1$, where N_f is the number of rocking raced framed per column line) or two rocking braced frames per column line ($N_f = 2$). The roof of the 2-storey buildings comprised a 76 mm deep bare steel deck, whereas a composite slab (65 mm thick concrete on top of 76 mm deep steel deck) was adopted for the roof of the 4- and 8-storey buildings and the floors of all buildings. The braced frame elevations are also shown in Figure 1 a. A chevron (inverted V) bracing was adopted for all frames.

Design loads and load combinations were as specified in the National Building Code (NBC) of Canada 2015 and the framing members were designed following the requirements of the CSA S16-19 Canadian steel design standard [14].The values of the dead loads (D), floor live load (L), and roof snow loads (S) used in the designs are given in Figure 1 a. The girders and beams at the roof and floor levels were designed under the load combinations 1.25 D + 1.5 S (roof) and 1.25 D + 1.5 L (floors), as prescribed in the NBC. Floor vibrations were verified using the criterion defined in AISC Design Guide 11 [15] assuming an office occupation. The natural frequency of the floors was equal to 4.6 and 4.08 Hz, respectively, for the interior and edge bays, assuming composite action and considering a weight equal to the dead load plus an expected live load of 0.53 kPa, as recommended for vibrational analysis.

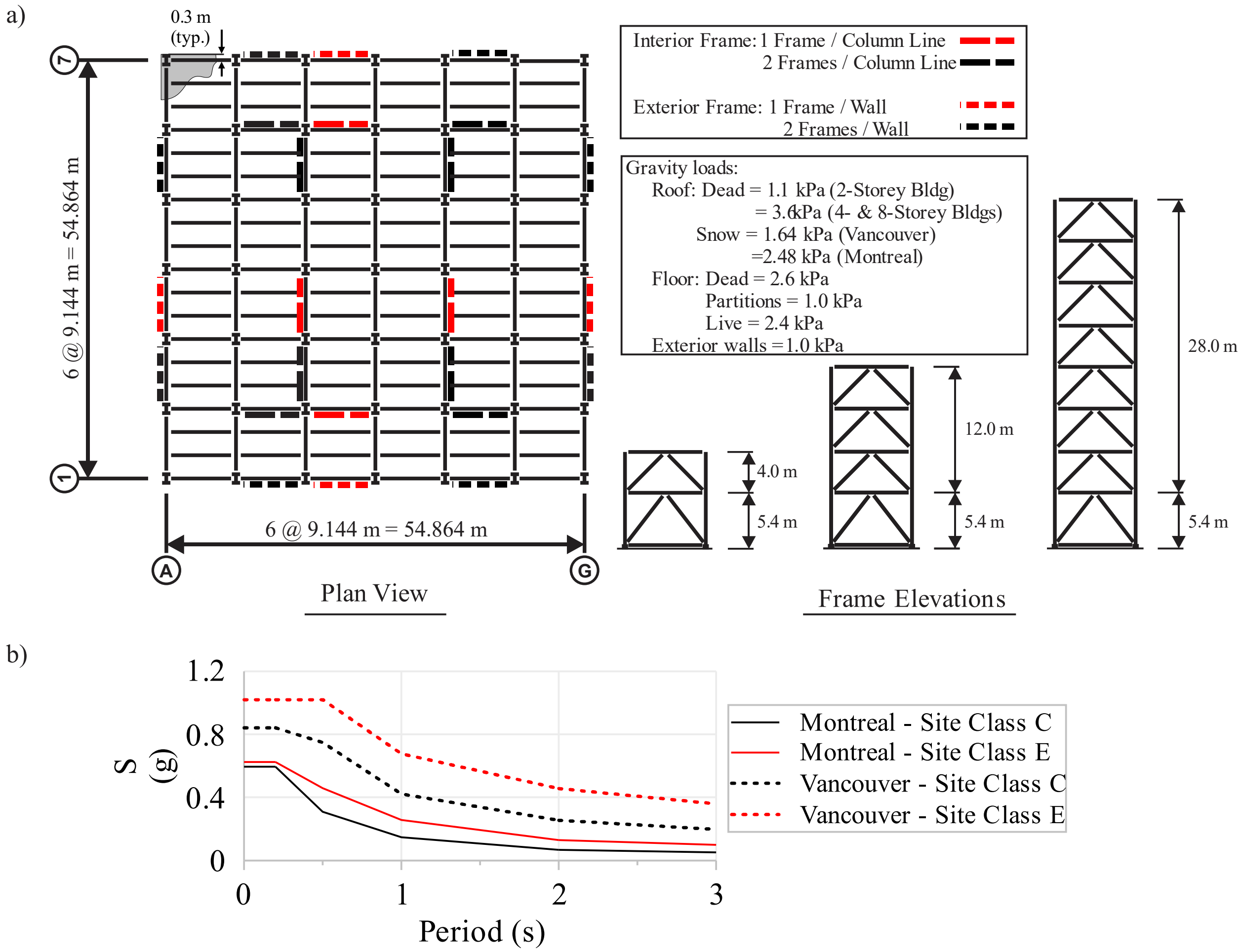

Figure 1 a) Structure plan view, design gravity loads and braced frame elevations of the buildings studied; and b) NBC 2015 Design Spectrum, $S(T)$.

Design seismic forces were obtained from response spectrum analysis (RSA) performed using the design spectrum, $S(T)$, prescribed in the 2015 NBC. This spectrum is obtained from linear interpolations between spectral ordinates determined for a probability of exceedance of 2% in 50 years and modified to account for local site conditions. Spectral ordinates for each location were obtained from Earthquakes Canada [16] and the design spectra are plotted in Figure 1 b. The RSA was performed with a numerical model that included only the horizontal masses representing the frame tributary seismic weight. Accidental eccentricity was not considered in the design. The seismic weight includes the dead load with a reduced partition load of 0.5 kPa, plus 25% of the roof snow load. The resulting total values of W are reported in Table 1. The values of the base shear from RSA, V_{RSA}, are given in Table 1. The design analysis has been performed independently in each of the two directions of the building.

Table 1 Properties of the structures studied (per frame)

Building ID	N_f	W (kN)	V_{RSA} (kN)	$M_{o,min}$ (kNm)	C_D (kN)	F_s (kN)	M_r (kNm)	Ω	R_{eff}	β	T_1 (s)	T_2 (s)	T_3 (s)
MC2E-R3.5	1	9695	340	2357	315	274	5388	2.29	3.5	0.93	0.559	0.252 (0.254)	-
VC2E-R8	1	9372	830	5613	315	299	5616	1.00	8	0.97	0.535	0.231 (0.233)	-
VC2I-R8	1	9372	833	5622	477	139	5629	1.00	8	0.45	0.533	0.226 (0.228)	-
MC4E-R3.5	1	27041	411	4897	910	313	11179	2.28	3.5	0.51	1.213	0.423 (0.438)	0.259 (0.262)
ME4E-R8	1	27041	683	8589	910	30	8592	1.00	8	0.06	1.213	0.423 (0.438)	0.259 (0.262)
ME4E-R7	1	27041	677	8534	910	157	9753	1.14	7	0.29	1.231	0.415 (0.429)	0.260 (0.269)
ME4E-R5	1	27041	689	8684	910	610	13895	1.60	5	0.80	1.175	0.407 (0.423)	0.253 (0.259)
ME4I-R5	1	27041	712	8980	1455	117	14373	1.60	5	0.15	1.131	0.387 (0.404)	0.239 (0.244)
VC4E-R8	2	13359	706	9115	910	88	9122	1.00	8	0.18	0.882	0.303 (0.313)	0.188 (0.193)
VC4E-R7	2	13359	713	9205	910	241	10521	1.14	7	0.42	0.875	0.303 (0.313)	0.187 (0.191)
VC4E-R6	2	13359	739	9553	910	483	12734	1.33	6	0.69	0.847	0.298 (0.308)	0.183 (0.185)
VC4E-R5	2	13359	752	9713	910	790	15541	1.60	5	0.93	0.838	0.291 (0.302)	0.179 (0.181)
VC4I-R6	2	13359	781	9969	1455	0	13303	1.33	6	0.00	0.807	0.281 (0.293)	0.175 (0.178)
VC4I-R3.5	2	13359	816	10698	1455	1219	24450	2.29	3.5	0.91	0.736	0.255 (0.265)	0.159 (0.164)
VE4E-R8	2	13359	1118	14691	910	698	14700	1.00	8	0.87	0.805	0.285 (0.296)	0.176 (0.178)
MC8E-R3.5	1	54041	422	7327	1876	0	17150	2.34	3.5	0.00	2.558	0.771 (0.786)	0.426 (0.438)
ME8E-R4	1	54041	802	15267	1876	1464	30537	2.00	4	0.88	2.229	0.657 (0.677)	0.359 (0.368)
ME8I-R4	1	54041	847	16534	2993	624	33077	2.00	4	0.35	1.979	0.607 (0.632)	0.336 (0.352)
VC8I-R6	2	26859	955	20600	2993	10	27463	1.33	6	0.01	1.499	0.447 (0.464)	0.244 (0.251)
VC8E-R8	2	26859	842	17807	1876	72	17809	1.00	8	0.07	1.782	0.532 (0.544)	0.298 (0.307)
VC8E-R6	2	26859	857	18287	1876	791	24383	1.33	6	0.59	1.740	0.525 (0.537)	0.296 (0.305)
VE8E-R8	2	26859	1503	34060	1876	1850	34067	1.00	8	0.99	1.522	0.456 (0.473)	0.250 (0.258)

The base rocking joints of the studied G-CRBFs buildings were then designed to resist the design overturning moment $M_{o,min}$ from:

$$M_{o,min} = \frac{M_{RSA}}{R_d R_o} \tag{1}$$

where M_{RSA} is the base moment from RSA, and R_d and R_o are respectively the ductility- and overstrength-related force modification factors for specific framing systems as defined in the NBC. Currently, R_d and R_o are not specified in the NBC for G-CRBFs. In this study, R_o was set equal to

1.0 as the G-CRBF system does not possess dependable overstrength beyond its base overturning moment resistance. Therefore, the product R_dR_o becomes R_d. and, for simplicity, R is used instead of R_d thereafter in the article. Based on the satisfactory response of G-CRBFs observed in past studies [5;6], a maximum value of R = 8.0 was tentatively adopted for initial design. The values of $M_{o,min}$ calculated with R = 8.0 are given in Table 1. In the NBC, the load combination including seismic effects is 1.0 E + 1.0 D + 0.5 L + 0.25 S. In this combination, the NBC requires that the companion loads L and S be excluded when they counteract the seismic actions. For instance, live and snow companion loads were not considered for overturning moment resistance. For each building, the required minimum of the activation force F_s of the ED elements could then determined to obtain a base resisting moment, M_r, from ED and column dead load, C_D, equal to $M_{o,min}$:

$$M_r = (C_D + F_s)L \ = M_{o,min} \tag{2}$$

where L is the width of the braced frame.

Values of C_D are given in Table 1, together with the selected F_s value. To ensure self-centring response, F_s had to be less than C_D. For most of the buildings in Vancouver, this could be satisfied by having two rocking braced frames per column line, as indicated by N_f = 2 in Table 1. For several buildings, the column load C_D was sufficient to resist alone $M_{o,min}$. This was the case when the design seismic loads were low (e.g., site class C in Montreal) and the frames were located along the interior column lines (larger C_D). These frames therefore inherently possessed a moment M_r higher than $M_{o,min}$ obtained with R = 8, resulting in a system overstrength $\Omega = \ M_r/M_{o,min}$ and an effective force modification factor $R_{eff} = 8.0\ /\Omega$. For these frames, the value of F_s was chosen to obtain R_{eff} values rounded to the nearest 0.5 value. Moreover, in order to obtain G-CRBF designs that could be easily compared, F_s was also selected to obtain the same R_{eff} among series of buildings. For instance, the MC8E-R3.5 building had R_{eff} = 3.5 without any ED (F_s = 0), and F_s for the 2- and 4-storey buildings for the same conditions (MC2E and MC4E) was adjusted to keep R_{eff} the same for all three structures. As discussed later, F_s was also varied intentionally for some of the buildings to study the influence of F_s and R_{eff} on the structure response. Once F_s was selected, the energy dissipation ratio of the frames, β [17], could be determined from:

$$\beta = 2\frac{F_S}{F_S + C_D} \qquad (3)$$

Values of M_r, Ω, R_{eff}, and β are given in Table 1, together with the periods of the building in their first 3 lateral modes. For periods T_2 and T_3, the values in brackets are the periods of the 2^{nd} and 3^{rd} modes of vibration of the frame in the uplifted condition. These periods are respectively referred to as $T_{u,2}$ and $T_{u,3}$ later in the article.

A friction ED device was chosen for this study, as this mechanism was shown to be most effective in controlling drifts in past studies [3;6]. Furthermore, reliable friction EDs can be easily implemented in practice and, eventually, inspected and replaced after an earthquake.

The braced frame members were then capacity-designed using member forces from superimposing the results of two response spectrum analyses (RSA) performed with the design spectrum *S*. The first RSA was performed on the fixed base frames to obtain member forces due to first mode response at the frame uplift. Therefore, only the first mode forces, $F_{E,1}$, were kept and were scaled by the ratio M_r/M_{RSA}. The second RSA was performed to obtain member forces from higher modes of vibration developing upon rocking. To perform this analysis, a low-stiffness vertical spring was introduced at the base of one of the braced frame columns to overcome the numerical issues associated with the loss of contact during column uplift [18]. The design spectrum was also truncated for periods longer that the second mode period to only include forces contributed by the second and higher modes, $F_{E,2}$, … $F_{E,n}$. These contributions were then combined using a modified

SRSS rule, as was done in [7]. The results were then corrected by the factor $R_{\xi} = (0.05/\xi)^{0.4}$, as prescribed in [19] to account for the fact that steel braced frames typically have less than 5% damping. A value of $\xi = 0.03$ was assumed for this correction, resulting in $R_{\xi} = 1.23$. The total design member forces, $F_{E,Total}$, were then obtained from:

$$F_{E,Total} = \frac{M_r}{M_{RSA}} F_{E,1} + \sqrt{F_{E,2}^2 + F_{E,3}^2 + \cdots + F_{E,n}^2}\, R_{\xi} \tag{4}$$

In NBC, gravity loads in the seismic load combination include 1.0 D + 0.5L + 0.25 S, and the gravity induced member forces were added to forces $F_{E,Total}$. Members were then designed in accordance with the requirements of the CSA S16 standard for axial compression (braces and columns) and for combined axial compression and moments (beams). The braces were ASTM 1085 HSS members (F_y = 345 MPa), whereas ASTM A992 W shapes (F_y = 345 MPa) were used for the beams and columns. All beam-to-column connections were assumed to be single shear-tab bolted connections with ASTM F3125 Grade A325M 25 mm bolts (threads excluded).

At the end of the design process, the drifts were checked to be less than the NBC limit of 2.5% h_s (h_s is the storey height). Peak storey drifts considering nonlinear effects (Δ_x) were determined using Eq. (5), which was proposed by Zhang et al. [20] for PT-CRBFs to account for the fact that the traditional equal displacement assumption is often not conservative for rocking structures.

$$\Delta_{x,predict} = \Delta_{xe} \times C_R \tag{5}$$

where Δ_{xe} is the lateral deflection determined from RSA of the fixed base frames and C_R is the displacement ratio computed from:

$$C_R = 1 + \frac{(R_{eff} - 1)^{0.515}(0.184 + 0.119(1 - \beta)^{1.173})}{T_1^{1.478}} \tag{6}$$

Values of C_R and $\Delta_{x,predict}$ with Eq. 5 are given in Table 2. As shown, all storey drifts are lower than the NBC limit.

The characteristics of the buildings were chosen in such a manner that it was possible to compare the response of two different buildings for which only one design parameter was varied. These parameters are the ED resistance F_s (and factor R_{eff}), the building height, the seismicity of the building location, the site class, and the location of the frames in the building. The reasons for investigating the influence of these parameters are summarized in the next paragraphs.

In the studied structures, the value of R_{eff} could be reduced by increasing the F_s value. Increasing F_s also leads to a higher energy dissipation capacity and the combination of a lower R_{eff} and higher F_s was expected to result in diminish the number and amplitude of the rocking excursions, and thereby, the structure lateral displacements. Limiting the rocking response was also expected to reduce member forces due to higher mode response as these forces are triggered by columns uplifting from and impacting against the foundations and develop more during rocking excursions. To study the possible combined effects of F_s and R_{eff}, buildings ME4E, VC4E and VC4I were selected, as it was possible for these structures to increase F_s so that R_{eff} would take values between 3.5 and 8, without exceeding C_D.

Buildings MCE-R3.5 and VCE-R8 were selected to study the influence of the building height on the seismic response of G-CRBFs. In both cases, buildings having 2, 4 and 8 storeys and designed with the same R_{eff} factors were used to verify if acceptable performance could be achieved for all heights and also study the variation of the effects of the floor framing vibrations over the height of the building.

Seismic ground motions in eastern Canada (Montreal) are expected to be richer in high frequencies and have shorter duration compared to those generated by the crustal and interface subduction earthquakes anticipated in the Vancouver region. Smaller building drifts were therefore expected for the eastern Canada site, and buildings VE4E-R8 and ME4E-R8 having the same heights and R_{eff} factors were selected to examine this possible effect. It is noted that due to higher seismic loads in Vancouver, the VE4E-R8 building was designed with a significantly higher amount of energy dissipation capacity compared to the one in Montreal (β = 0.87 vs 0.06) to obtain the same R_{eff}. This difference in ED could therefore possibly offset to some extent the difference in ground motion effects.

Buildings VC4E-R8, VE4E-R8, VC8E-R8 and VE8E-R8 were selected to study the influence of the site class on the seismic response. In that case, higher displacement and force demands were expected for the buildings on site class E. However, these buildings were designed for higher seismic loads than their site class C counterparts and were therefore conferred higher F_s and β values to achieve the required base moment resistance: β = 0.87 vs 0.18 for the 4-storey buildings, and β = 0.99 vs 0.07 for the 8-storey building. A similar comparison was not possible for Montreal because it was not possible to obtain F_s values lower than C_D such that buildings on site classes C and E would have the same R_{eff} factor.

Buildings ME4-R5, ME8-R4, VC2-R8, VC4-R6, and VC8-R6 were chosen to assess the influence of the braced frame location in the building on the G-CRBF seismic response. The focus was put on comparing the effects of column impacts, as larger tributary masses are mobilized during rocking excursions in inner G-CRBFs. For these buildings, the value of R_{eff} was governed by the frames along interior column lines due to the higher weight they support, and higher ED capacity was required for the G-CRBFs located on exterior column lines.

3. Numerical Modelling

A numerical 3D-model of the frames was created with Opensees [11] to include the gravity system present in the bays adjacent to the rocking braced frames. Elastic response of the braced frames was expected because of the design method. Hence, the frame members were modelled using truss elements for the braces and columns and elastic beam-column elements for the beams. In the analyses, only the dead load (1.0 D) was applied to the models so that the frame base overturning resistance in the models was same as that considered in design (C_D only). Floor live loads and roof snow loads were therefore not included. Floor and roof beams framing into the G-CRBFs were modelled using 6 elastic beam elements, and vertical point loads and vertical masses corresponding to 1.0 D were assigned to all nodes along these beams. High vertical accelerations were expected in the floor and roof systems, and it was assumed that the steel beams supporting a concrete slab would not behave compositely with the slab under the resulting high flexural demand. Steel beams were then modelled using bare steel properties. The resulting natural frequency of the floors under dead load only was 2.5 Hz. For the roofs, the frequencies were 4.5 Hz and 2.3 Hz, respectively, for the 2-storey buildings with bare steel deck panels and the 4- and 8-storey buildings with a roof slab. The bolted shear beam-to-column and beam-to-girder connections were modelled as pinned, using equal degree of freedom constraints except for the in-plane rotation. In the complementary analyses detailed in Section 5.2, rotational springs with high stiffness and elastic-perfectly plastic hysteresis defined with a moment capacity corresponding to that resulting from all bolts reaching their slip resistance were introduced to account for the energy dissipated by friction in these connections, as suggested in [21]. For rotational springs, the slip force F_{slip} of a single bolt was computed according to [14] assuming a class A surface and A325 high-strength bolts. Two cases were studied with this model: a first, upper bound, case for which the rotational moment capacity of the springs was based on a bolt slip resistance equal to 1.0 F_{Slip} (referred to as RS = 1.0); and a second case for which slippage was set equal to 0.3 F_{Slip} to mimic friction in snug-tightened bolts (RS = 0.3).

For all frames, the rocking interfaces were modelled using zero-length vertical compression-only (gap) links calibrated with past experimental studies [8, 22]. Horizontal gap links were added at the rocking interface to simulate the horizontal blockers installed at the rocking column bases. The energy dissipating elements were included at the base of the rocking columns using zero-length link elements having an elastic-perfectly plastic response with a yield force equal to F_s. Accounting for energy dissipation upon impact of the column against its foundation is beyond the scope of this paper.

At each storey level, the tributary seismic weight of the frame was assigned as a horizontal mass to the joint at the beam mid-span. To account for global P-Delta effects, a pinned leaning column was added to the model. At each storey level, the lateral displacement of the leaning-column node was constrained to be the same as the lateral displacement of the frame joint located at the beam mid span in the braced frame. The vertical loads applied on the leaning column was equal to the frame tributary gravity loads reduced by the loads already applied on floor and roof beams framing into the braced frames.

Damping was specified as Rayleigh mass- and initial stiffness-proportional damping computed with coefficients calculated to obtain 3% of critical damping in lateral modes 1 and 2 for the 2- and 4-storey buildings and lateral modes 1 and 3 for the 8-storey buildings. Damping was only applied to the frame members, but not the rocking interface elements. Nonlinear response history analyses were run using a Newmark integration scheme and a Krylov-Newton algorithm. The time steps in the analyses were equal to one quarter of the ground motion time steps. Second-order geometric (P-Δ) effects were considered in all analyses.

4. Response History Analysis

The building structures were subjected to an ensemble of representative ground motions selected and scaled in accordance to Method A in the NBC User's Guide [23]. For the buildings in Montreal, the ensemble of ground motions consisted of two suites of simulated ground motions corresponding to two sources of earthquakes dominating the seismic hazard in eastern Canada: 5 ground motions from M6.0 earthquakes at short distances for short period excitations and 6 ground motions from M7.0, more distant earthquakes contributing to long-period demands, as documented by Atkinson [24]. For Vancouver, the ground motion ensemble consisted of three suites of five ground motion records, each suite corresponding to one of the three sources of earthquakes contributing to the hazard in southwest British Columbia: shallow crustal earthquakes, in-slab subduction earthquakes and interface subduction earthquakes. As the fundamental period of the buildings varied with the structure heights and locations, ensembles of ground motions were created and scaled for the period range of interest specific to each building height and location.

4.1. Overall Response

The envelope of peak storey drifts, Δ_x/h_s, as well as peak horizontal accelerations in the frame, a_h, are presented in Figure 2 for buildings VC2I-R8, VC4E-R8, and ME8E-R4, for these three buildings cover the variety of design parameters studied. In the figures and for all the results presented hereafter, the design seismic demand (darker and thicker line in the figures) corresponds to the mean of the five largest peak values obtained for the ensemble of ground motions, as defined in the NBC User's Guide. In the rest of the paper, the analysis results that are reported for the different response parameters correspond to design seismic demand values. As shown, for the three buildings presented, peak storey drifts lie between 1.0 and 2.25% h_s over the building heights. The storey drifts also remain the same over the building height, indicating the dominance of rocking response on the structure displacements. For all three buildings, horizontal accelerations lie between 0.45 and 0.75 g. In Figure 2a and 2b, a_h = 0.75 g at the roof level of the two buildings located in Vancouver on a class C site. In Figure 2c, a_h at the roof is 0.64 g for the building on a site class E in Montreal. These two values compare well with the horizontal accelerations that must be used at the roof level for determining design forces for non-structural components and equipment in the NBC: 0.76 and 0.56 g, respectively, for Vancouver and Montreal. This suggests that buildings with G-CRBFs are not expected to sustain peak horizontal accelerations larger than those expected with conventional seismic force resisting systems. Even though some variations are observed, peak horizontal accelerations also are of similar magnitude over the height of the buildings.

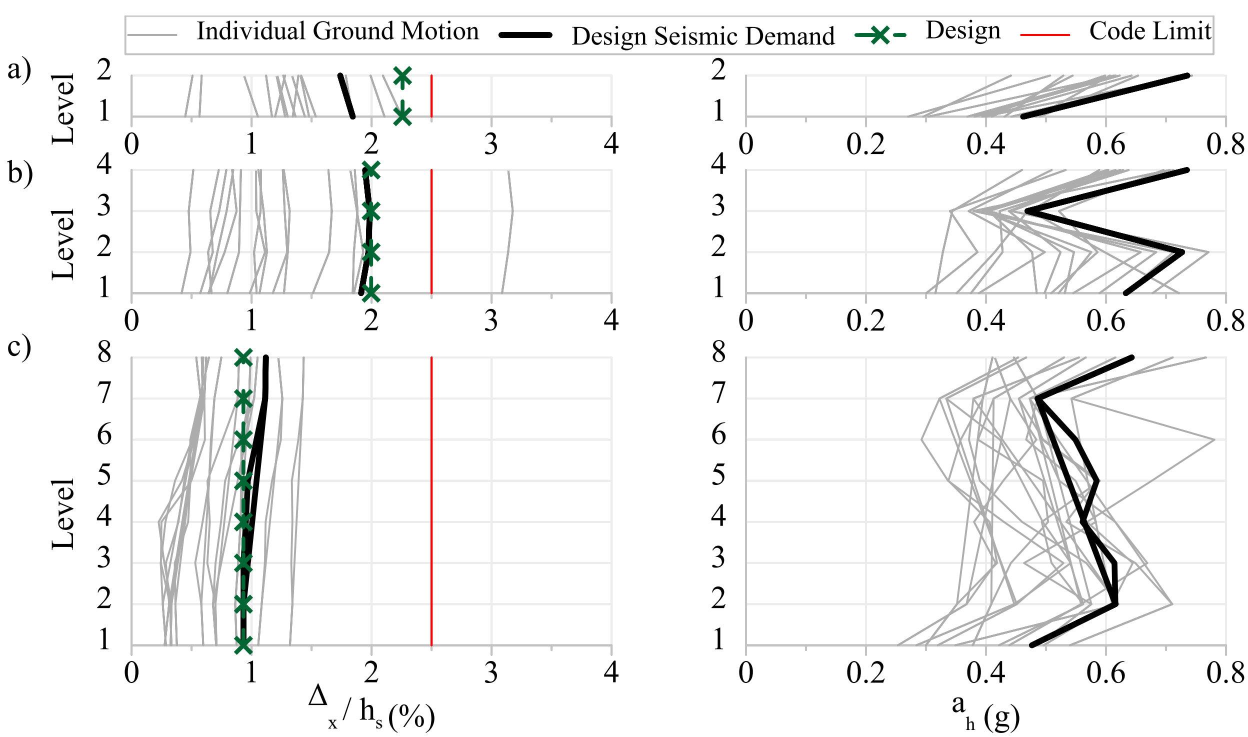

Figure 2 Peak storey drifts and peak horizontal accelerations for Buildings: a) VC2I-R8; b) VC4E-R8; and c) ME8E-R4.

Table 2 Analysis Results

Building ID	β	C_R	$\Delta_{x,predict}$ (%)	Δ_x/h_s (%)	Uplift (mm)	a_h (g)	r_{Br}	$r_{Col,floor}$	Moment (kNm)	Shear (kN)	$S(T_1)$ (g)	$S_{5GM}(T_{u,2})$ (g)	$\hat{\beta}_{RTR}$	$\hat{S}_{CT}$	P(*IM*=1) (%)
MC2E-R3.5	0.93	1.72	0.60	0.48	31	0.43	0.98	0.82	105	34	0.29	0.46	0.43	11.05	0
VC2E-R8	0.97	2.28	1.91	1.67	137	0.71	1.02	0.96	231	77	0.73	0.88	0.45	7.45	0.01
VC2I-R8	0.45	2.67	2.26	1.84	151	0.74	1.06	1.12	282	96	0.73	0.82	0.6	10.10	0.03
MC4E-R3.5	0.51	1.28	0.62	0.7	44	0.46	1.09	0.93	54	18	0.13	0.42	0.51	5.48	0.21
ME4E-R8	0.06	1.6	1.34	1.88	148	0.57	1.22	0.96	107	35	0.23	0.57	0.62	5.47	0.67
ME4E-R7	0.29	1.49	1.43	1.61	122	0.57	1.17	0.95	90	30	0.23	0.58	0.57	5.34	0.46
ME4E-R5	0.8	1.32	1.11	1.23	74	0.61	1.12	0.93	75	25	0.23	0.5	0.4	5.05	0.06
ME4I-R5	0.15	1.48	1.21	1.21	85	0.6	1.09	0.89	93	31	0.24	0.59	0.5	7.18	0.04
VC4E-R8	0.18	1.91	2.00	2.05	169	0.73	1.22	1.06	199	68	0.5	0.73	0.38	6.01	0.01
VC4E-R7	0.42	1.76	1.77	1.56	125	0.77	1.21	1.02	170	57	0.5	0.75	0.33	4.00	0.1
VC4E-R6	0.69	1.63	1.52	1.4	109	0.75	1.16	0.99	141	46	0.52	0.8	0.32	3.66	0.15
VC4E-R5	0.93	1.5	1.43	1.18	87	0.73	1.09	0.96	122	41	0.53	0.69	0.36	5.61	0.01
VC4I-R6	0	1.95	1.79	1.83	144	0.79	1.2	0.94	174	59	0.55	0.84	0.44	5.40	0.08
VC4I-R3.5	0.91	1.48	1.23	0.93	60	0.85	1.1	0.94	127	42	0.59	0.94	0.49	5.36	0.17
VE4E-R8	0.87	1.73	2.20	1.93	158	0.85	1.05	0.91	187	63	0.81	0.8	0.53	4.73	0.52
MC8E-R3.5	0	1.12	0.62	1.02	62	0.49	1.04	0.91	45	15	0.06	0.24	0.4	6.54	0.01
ME8E-R4	0.88	1.1	0.93	1.12	64	0.65	1.25	1.03	92	31	0.12	0.41	0.52	5.32	0.28
ME8I-R4	0.35	1.16	0.84	1.2	77	0.62	1.16	0.96	71	24	0.13	0.39	0.45	3.56	0.93
VC8I-R6	0.01	1.38	1.41	2.44	203	0.85	1.17	0.99	123	41	0.34	0.67	0.82	7.32	1.1
VC8E-R8	0.07	1.34	1.72	2.47	196	0.77	1.15	0.99	103	34	0.29	0.6	0.71	5.43	1.59
VC8E-R6	0.59	1.23	1.55	1.87	144	0.77	1.13	0.97	91	30	0.3	0.54	0.67	6.27	0.72
VE8E-R8	0.99	1.27	2.21	2.24	181	1.07	1.33	1.16	140	48	0.56	0.99	0.54	4.30	0.89

Table 2 presents the results of the analyses performed for the 22 buildings studied. For Δ_x/h_s and a_h, the maximum values over the height are given. Note that storey drifts for the *Para* and *Perp* configurations were almost same (less than 1% difference) and the maximum results are presented. As shown, peak storey drifts vary between 0.48% and 2.47% h_s: the G-CRBF system with proper combinations of F_s and R_d values can meet the NBC limit of 2.5% . Higher drifts were obtained for higher values of R_{eff} and lower values of β. These trends were expected from Eq. (6). Figure 3a shows the evolution of the ratio between the Δ_x/h_s values of Table 2 and the predictions from Eq. 6 as a function of β.

As shown, predictions are better when β increases. For $\beta > 0.4$, the ratios vary between 0.82 and 1.1, with a mean value of 0.96. In Figure 3b, an excellent correlation is found between the maximum storey drifts and the frame angles from column uplift, confirming that peak storey drifts are mainly governed by the first mode response of the frames upon rocking.

In Table 2, the values of a_h for all buildings lie between 0.43 g and 1.07 g. No significant difference was found between the horizontal acceleration obtained for the configurations *Para* and *Perp*. For all cases considered, the a_h values are higher in Vancouver than in Montreal, and for buildings located on site class E than site class C. Horizontal accelerations are reduced when increasing R_{eff} for a given building configuration, which is expected due to lower forces associated to higher R_{eff}. Figure 3c presents the values of a_h normalized with respect to the design spectrum ordinate at a period of 0.2 s, *S*(0.2 s). This period was chosen because a_h is largely induced by elastic higher mode response, typical of this framing system, which mainly depends on the high frequency content of the ground motion characterized by *S*(0.2 s). A good correlation between ah and *S*(0.2 s) was also noted in this study. The figure shows that *S*(0.2 s) could be used to predict a_h for all buildings. This good correspondence also suggests that a_h is mainly governed by higher mode response.

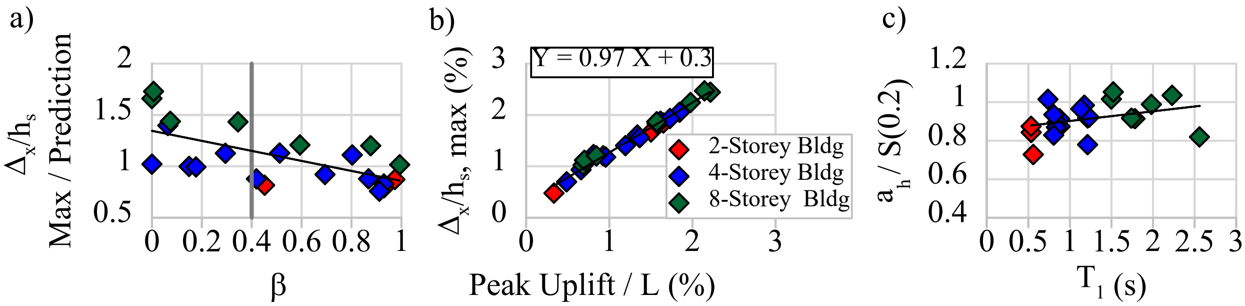

Figure 3 Overall results for all G-CRBFs: a) Ratios between observed maximum storey drifts and predicted storey drifts; b) Evolution of maximum storey drifts as a function of frame base rotation from column uplift; and c) Normalized peak horizontal accelerations.

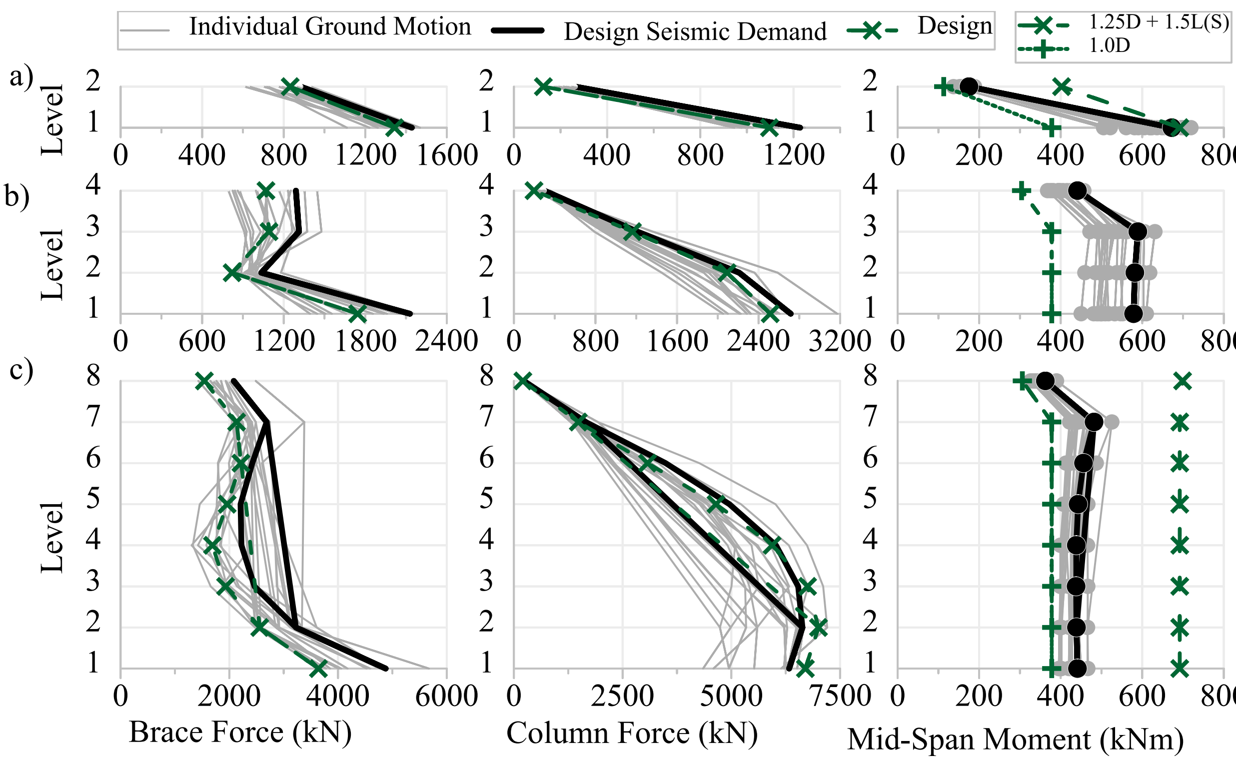

Figure 4 Peak axial forces in the braced frame braces and columns, and peak moments at mid span of the out-of-plane beams in Buildings: a) VC2I-R8; b) VC4E-R8; c) and ME8E-R4.

Peak axial loads in the braces and columns of the three buildings of Figure 2 are presented in Figure 4. The figure also presents peak flexural moments at mid-span of the beams framing perpendicular to the G-CRBF, referred to herein as the out-of-plane beams. Peak brace axial loads are slightly underestimated by the design procedure, whereas peak column axial loads are accurately estimated. Higher mode effects on member forces are observed for the 4- and 8-storey buildings.

Close examination of the results from the analyses conducted in both orthogonal building directions showed that the brace axial forces are slightly larger, by 3% on average, for the *Perp* configuration compared to the configuration *Para*. This small increase is due to the secondary floor beams that are supported by the beams of the rocking braced frame in the *Perp* configuration. These secondary beams induce additional axial loads in the braces when dynamically oscillating in the vertical direction. In contrast, the axial loads in the columns are slightly larger, by 2% on average, for the *Para* configuration.

In Figure 4, peak moments in the out-of-plane beams have comparable amplitudes throughout all floor levels for all three buildings. This is expected as dynamic magnification of beam moments is mostly due to column uplift and this source is same at all storeys. As also shown, peak beam moments decrease as the building height is increased. This effect will be discussed further later. In Figure 4, moments from static gravity loads are also presented for the load combinations 1.0 D and 1.25 D + 1.5 L (or 1.25 D +1.5 S at the roof level). The second load combination was used to design the beams. Peak moments under ground motions lie between the two static values, which suggests that, for these three buildings, frame rocking would not trigger yielding of the floor and roof beams if only 1.0 D is present during the earthquake.

Figure 5 presents the average values over the building height of the ratios r between observed and predicted (design) axial loads in the braces (r_{Br}) and columns (r_{Col}) for all buildings. The results are plotted as a function of R_{eff} and the values of r_{Br} and $r_{Col,floor}$ are reported in Table 2. In Figure 5a, Brace axial loads are generally underestimated compared to the design values, with a mean r_{Br} of

1.14 for all buildings. This is attributed to the additional vertical inertia forces induced in the frame from the dynamic response of the floor and roof framing systems. Higher values of r_{Br} were observed in the buildings with a higher R_{eff}, which suggests that these additional forces can be higher for frames experiencing more frequent and longer rocking excursions, as this can favor the development of more pronounced higher mode effects. Figure 5b displays the ratio between observed and predicted column axial loads at floor levels $r_{Col,\ Floor}$, whereas Figure 5c shows $r_{Col,\ Roof}$. As shown, the column axial loads at floor levels are accurately predicted by the design procedure, with $r_{Col,\ Floor}$ ranging from 0.82 to 1.16 with a mean value of 0.97. Conversely, $r_{Col,\ Roof}$ values lie between 1.0 and 2.77, which suggests unconservative design at this level. In chevron bracing, lateral seismic loads do not induce column axial loads at the top level, and these rCol, Roof values reflect the vertical dynamic response of the roof beams supported by the columns, as described in [6]. For the buildings studied, however, the high values of $r_{Col,\ Roof}$ would have no consequences because the same column section is used in the top two storeys, and the design of the columns would still be governed by axial loads in the second last level.

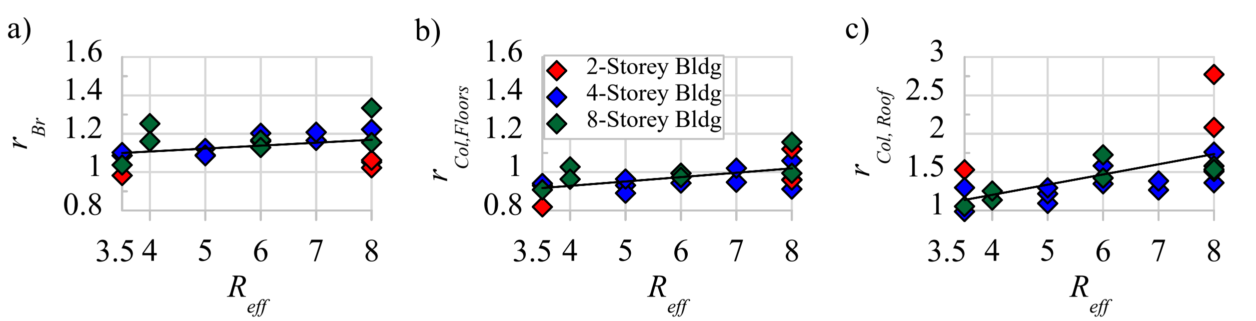

Figure 5 Ratio of the peak axial loads to design axial loads in: a) braces; b) columns at the floor levels; and c) columns at the roof level.

Figure 6 presents the ratio between observed and predicted axial loads in the braced frame members. In this case, the vertical masses corresponding to the weight of the floors and roof supported by the frame were included in the RSA used during the design. When comparing the results of Figure 5 and 6, it is observed that including vertical lumped masses at beam-column nodes in RSA had a limited influence on r_{Br} and $r_{Col,Floor}$ for the 4- and 8-storey buildings. A slight decrease of r_{Br} and $r_{Col,Floor}$ is noticeable for the 2-storey buildings. These results suggest that the influence of the vertical masses carried by the frame tends to decrease as the building height rises, as was discussed in [9]. This also suggests that a 2D-RSA that does not include the vertical mass tributary to the columns is appropriate for the design of mid-rise G-CRBF buildings. Only the $r_{c,roof}$ values are significantly improved by including the vertical masses in the analysis, as shown in Figure 6c.

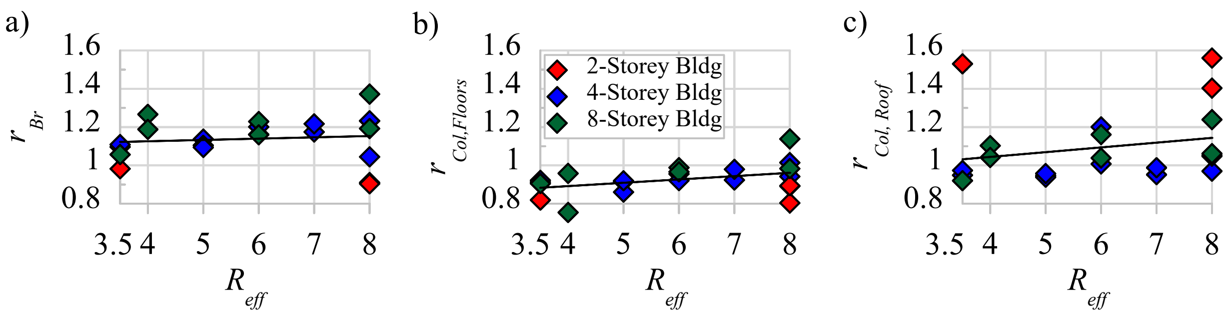

Figure 6 Ratio of the peak axial loads to design axial loads, vertical masses included: a) in the Braces ; b) in the Columns at the floor levels; and c) in the Columns at the roof level

Table 2 presents the peak dynamic moments and shears in the out-of-plane beams for all buildings. These peak values were obtained by subtracting from the peak values from time history analysis the static shears and moments from dead load. The values of $S(T_1)$ and $S_{5GM}(T_{u,2})$ are also presented in the table. The latter is the mean spectral value of the 5 ground motions contributing to the design seismic demand on the beams at the frame period $T_{u,2}$. The results show that peak dynamic moments increase as the building height decreases, with average values of respectively 596, 518 and 485 kN-m for the 2-, 4- and 8-storey buildings. Figure 7 shows that a nearly perfect correlation exists between peak dynamic shears and moments. The figure also shows a good correlation between peak column uplift amplitudes, $S(T_1)$ and $S_{5\,GM}(T_{u,2})$ with the peak dynamic moments, suggesting that peak dynamic beam moments and shears can be predicted using the design spectrum values at the periods T_1 or $T_{u,2}$.

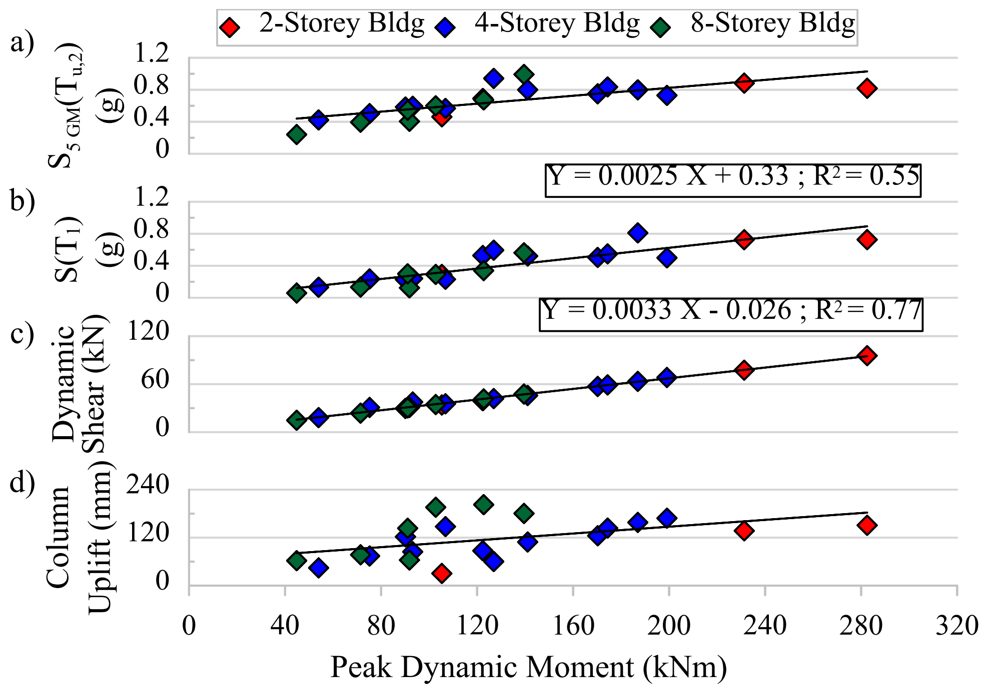

Figure 7 Evolution of key parameters as a function of the peak dynamic moments in out-of-plane beams for all buildings: a) $S_{5GM}(T_{u,2})$; b) $S(T_1)$; c) Peak dynamic shears; and d) Column Uplifts.

4.2. Influence of R_{eff}

The effect of R_{eff} on member force predictions was discussed in Figure 5. The influence of R_{eff} on frame response is further investigated in Figure 8 for one series of 4-storey buildings for which R_{eff} was varied from 3.5 to 8.0. Similar trends were obtained for the three other series of identical buildings having different R_{eff} values.

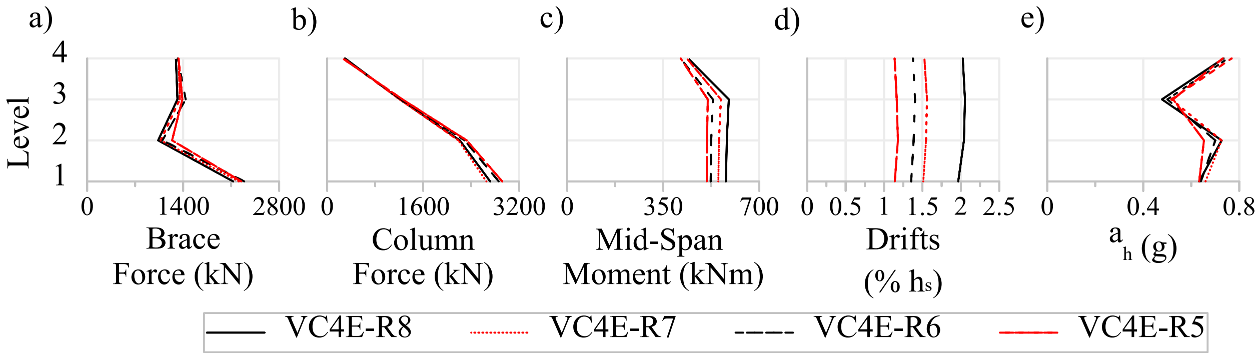

Figure 8 Influence of R_{eff} on: a) Brace axial loads; b) Column axial loads; c) Mid-span moments in the out-of-plane beams; d) Storeys drifts; and e) Peak horizontal accelerations.

Figure 8a shows that brace axial loads slightly increase as R_{eff} is decreased. As expected, storey drifts reduce when using a lower R_{eff} because a reduced R_{eff} comes with an increased energy dissipation β that helps control rocking response and lateral displacements. Similarly, beam moments decrease when R_{eff} is reduced because of the less pronounced rocking that results in lower column uplifts (as was shown in Table 2) and less severe column impacts. In contrast, R_{eff} does not seem to affect the value of a_h in Figure 8e.

4.3. Influence of the Building Height

Figure 9 details the response behaviour of two series of three buildings with different heights,3 buildings in Montreal and 3 buildings in Vancouver. However, as R_{eff} is significantly different for the buildings in Montreal and Vancouver, no comparison between the results obtained should be drawn. As shown from Figure 9 a and b, higher mode effects are noticeable in the peak axial loads in braces and columns at the upper levels of the 4- and 8-storey buildings. As the building height rises, the relative influence of higher modes effects increase, as was detailed previously [3]. From Figure 9c, the peak moment demands decrease as the building height increases, as explained in 4.1. From Figure 9d, the peak drifts are noticeably increased as the building height rises, for all buildings. From Figure 9e, as explained in 4.1, no significant influence of the building height is noticeable on the values of a_h.

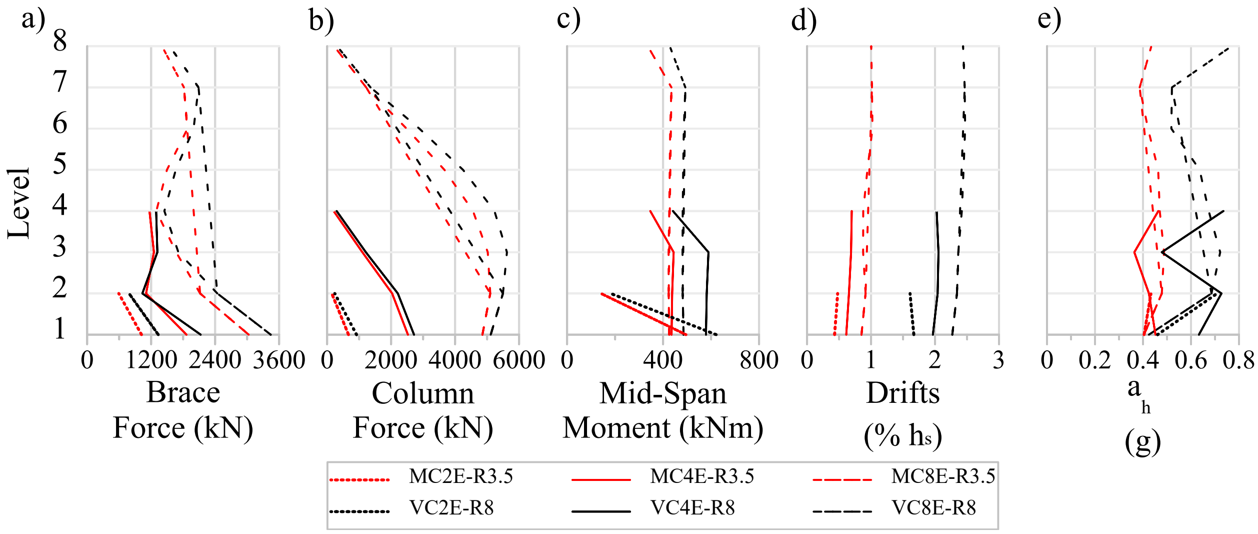

Figure 9 Influence of the building height: comparison of the response behaviour of buildings MCE-R3.5 and VCE-R8 for 2-, 4- and 8-storey buildings : a) Brace axial loads; b) Column axial loads; c) Mid-span moments in the out-of-plane beams; d) Storey drifts; e) Peak horizontal accelerations

4.4. Influence of the Seismicity

Responses of buildings ME4E-R8 and VE4E-R8 are compared to examine the influence of the seismicity on the peak drifts. The values of Δ_x/h_s for the building located in Montreal (comprised between 1.78% and 1.88%) were found to be very similar to the one located in Vancouver (comprised between 1.89% and 1.93%). The peak drifts could be kept the same for the two buildings, even if the Vancouver building was subjected to much more displacement demand compared to the one in Montreal. This was attributed to the higher ED capacity conferred to the building located in Vancouver. This shows that friction ED can be very effective in controlling displacements and storey drifts.

4.5. Influence of the Site Class

Figure 10 presents the results of the analyses performed on 4 buildings located in Vancouver to evaluate the influence of the site class on the G-CRBF seismic response. As expected, member forces and horizontal accelerations are higher for the two structures on a site class E. Slightly larger peak drifts are observed for the buildings located on site class C, which is attributed to the fact that higher ED capacity was conferred to the buildings located on site class E, thus resulting in a better control of drifts. It is expected that larger drifts would have been obtained for buildings located on site class E, has a similar β been assigned to buildings located in site class C. Finally, no significant influence of the site class on the values of r_{Br} and $r_{Col,floor}$ was noticed from Table 2, showing that the design method used can predict equally well the members forces in both locations.

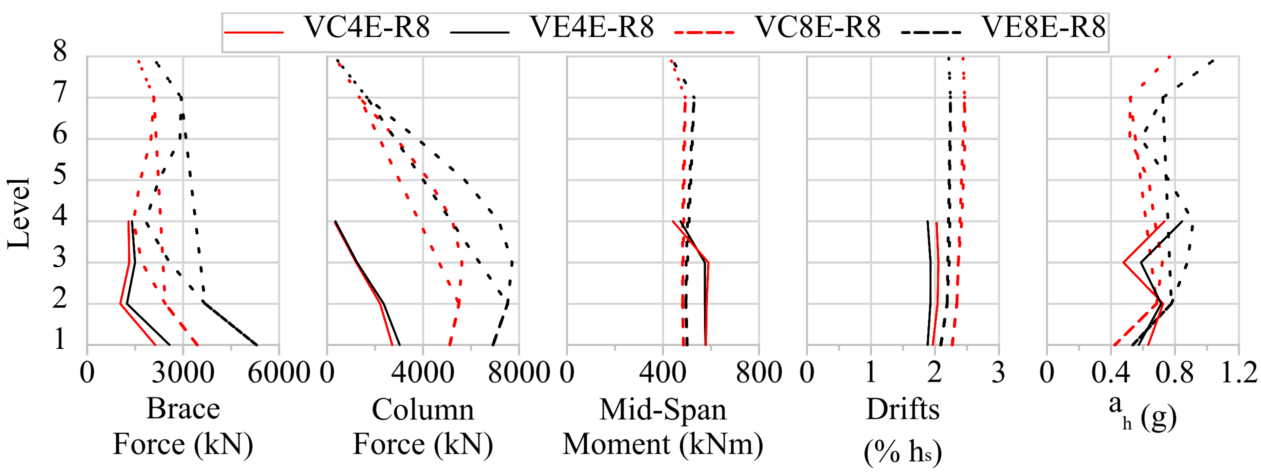

Figure 10 Influence of the site class on: a) Brace axial loads; b) Column axial loads; c)Mid-span moment in the out-of-plane beams; d) Storey drifts; e) Peak horizontal acceleration a_h

4.6. Influence of the Braced Frame Location

Figure 11 details the analysis results for buildings VC2-R8, ME4-R5 and ME8-R4 that are used to examine the influence of the location of the G-CRBFs in the buildings. Two other buildings configurations have been studied for the same purpose, and the results are similar to the ones presented herein.

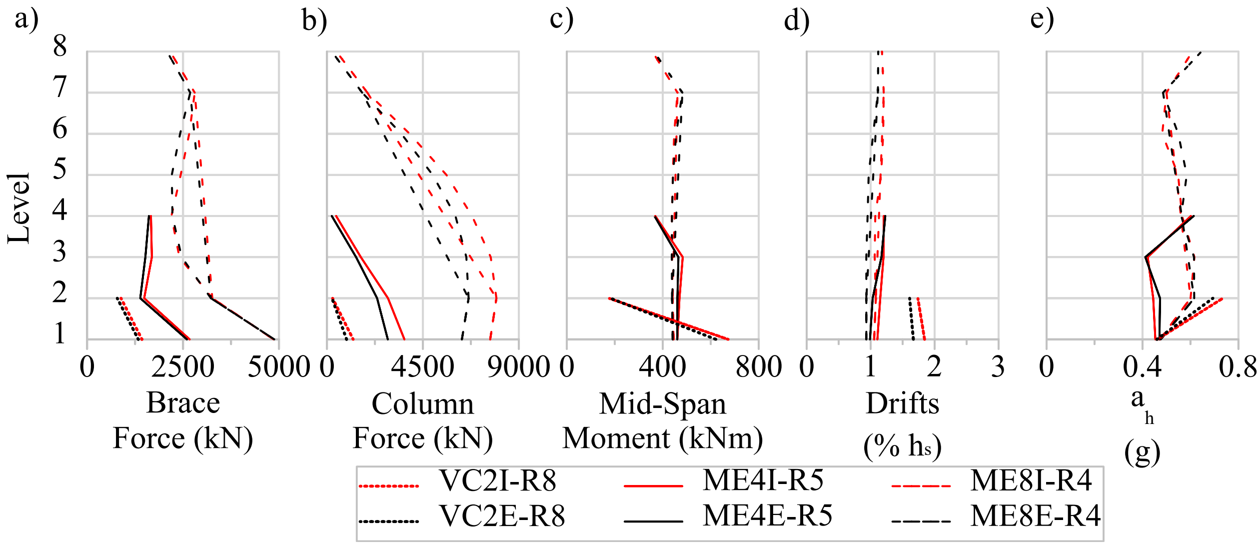

Figure 11 Influence of braced frame location on: : a) Brace axial loads; b) Column axial loads; c) Mid-span moment in the out-of-plane beams; d) Storey drifts; and e) Peak horizontal accelerations

As shown, the brace axial loads are slightly larger for braced frames located within the building. As expected, higher the column axial loads are observed in the inner braced frame, due to higher gravity loads carried by the columns. From Figure 11c, slightly higher drifts are noticeable for buildings with G-CRBFs along inner column lines, which is attributed to the lower energy dissipation capacity of these frames compared to those placed on the building exterior walls. Finally, no significant difference is observed for the peak beam moments, storey drifts, and horizontal accelerations. Overall, the location of G-CRBFs did not seem to affect much the seismic response of the buildings, suggesting that both locations would represent acceptable solutions. However, G-CRBFs on exterior column lines will likely require with EDs with higher F_s resistances to develop the design base moment resistance, which should result in a more effective drift control. Finally, from Table 2, no significant influence of the braced frame location of the values of r_{Br} and $r_{Col,floor}$ was noticeable, suggesting that the prediction of member forces is equally good at both braced frame locations.

5. Complementary Analyses

The study included a series of complementary analyses to investigate the influence of the vertical component of the ground motions on G-CRBF response and the possible beneficial effects of the energy dissipated by friction in the bolted beam-to-column connections.

5.1. Effects of the Vertical Component of the Ground Motions

The previous analyses showed that the vertical response of the gravity framing system did not significantly affect the seismic behaviour of the G-CRBFs buildings. In this section, the results from analyses including the vertical component of the ground motions are examined if those could increase the demands on the floor and roof beams. The analyses were performed for buildings in Vancouver as ground motion records from historical earthquakes were only available for this location. For consistency, the scale factors used for the horizontal ground motion components were also used for the vertical components, and both components were simultaneously applied to the model during the analysis. The study was conducted for buildings VCE-R8 (2-, 4-, and 8-storeys) and VEE-R8 (4- and 8-storeys) to cover the two site classes. Figure 12a presents the results obtained for the two 4-storey buildings, as they were representative of all the results. The results show that member axial loads, storey drifts and horizontal accelerations are all slightly increased (less than 5%) when considering the vertical component of the ground motions. However, an increase of up to 16 % is observed for the moments in the out-of-plane beams supported by the G-CRBFs, for all buildings studied. For this 4-storey building, the additional demands were slightly higher for site class C compared to site class E, as the vertical ground motions for the former have higher spectral accelerations in the period range of the floor and roof systems. Moments due to the load combination 1.25 D + 1.5 L (or 1.5 S) used in the design of the beam are shown in the figure, and it is seen that these moments were reached and exceeded even if only 1.0 D was considered in the analyses. For the 8-storey buildings, peak beam moments were of the same magnitude for both site classes. For the buildings in Figure 12, the analysis with the vertical ground motion components was repeated with the gravity loads from the load combination 1.0 D + 0.5 L + 0.25 S. In these analyses, the peak beam moments exceeded by 20 % the static moments from the design load combination 1.25 D + 1.5 L (or 1.5 S). This additional forces in floor and roof beam members should therefore be considered in their design.

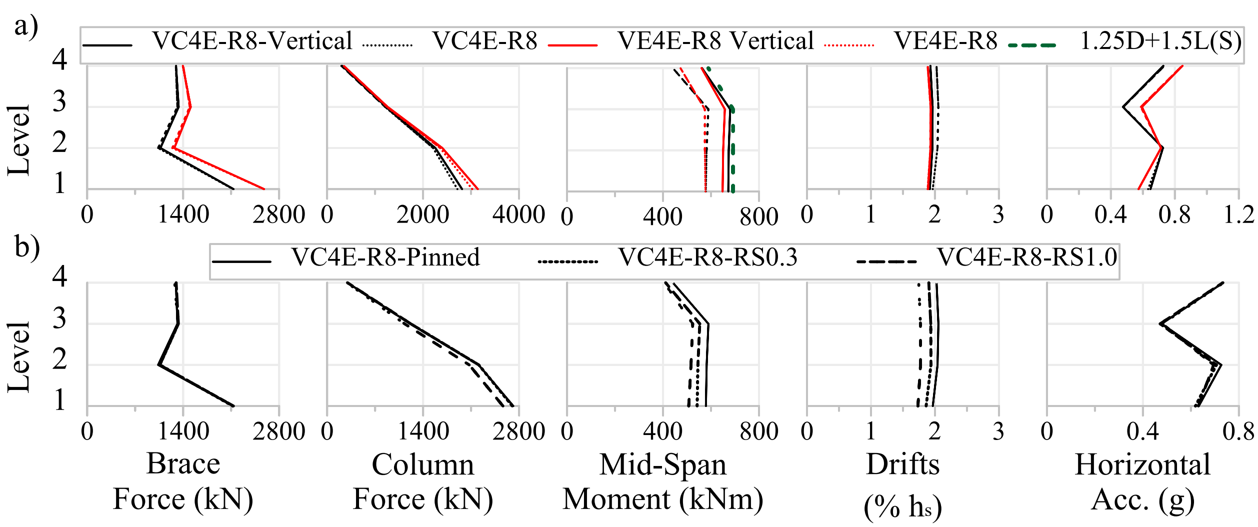

Figure 12 Results from complementary analyses: a) Influence of the vertical component of the ground motions (results with and without vertical ground motions are represented with solid and dotted lines, respectively); and b) Influence of the friction in bolted beam-to-column connections.

5.2. Effect of the Energy Dissipated at Beam-to-Column Connections

The effect of the additional energy dissipation capacity resulting from the friction resistance present in bolted beam-to-column connections were examined for building VC4E-R8. The results, presented in Figure 12b, show that axial loads in braces and columns were slightly reduced (< 5%) when considering the friction at beam-to-column connections. Beam moments were reduced by 7% and 14%, respectively, for RS = 0.3 and 1.0, compared to the results from the model with pinned beam connections. Peak storey drifts were reduced by 7% and 17%, respectively, for RS = 0.3 and RS=1.0, but peak horizontal accelerations remained unchanged. These results indicate that friction in beam-to-column can have beneficial effects on the seismic response of G-CRBFs.

6. Incremental Dynamic Analysis and Collapse Risk Assessment

Collapse fragility curves were generated to assess the seismic performance of the buildings listed in Table 1, following a methodology adapted from the procedure described in [25]. The focus of the investigation was to determine the margin against collapse resulting from G-CRBF overturning, which may represent a concern when considering that self-centering of the frames is provided solely by gravity loads. First, a truncated incremental dynamic analysis (TIDA) [26;27] was performed on each building using the numerical models and ground motion ensembles described in Section 3. The ground motions were scaled by successive increments of 25% to 50% of their initially scaled amplitudes until at least half of the records of the ensemble caused collapse. Buildings were considered to have collapsed when the peak measured storey drift exceeded 5%. The 5% storey drift threshold value was chosen at it corresponds to the maximum storey drift beyond which failure would be expected in the beam-to-column connections of the structures. In the models, the braced frame members were represented by elastic truss and beam elements and failure of members were therefore not considered. Using the work of Baker [27], the median collapse intensity $\hat{S}_{CT}$ and the record to record variability $\hat{\beta}_{RTR}$ were then estimated from the results of the TIDA, as depicted in Figure 13, instead of using β_{RTR}= 0.4 as suggested in [25]. In Figure

13, the intensity measure *IM* = 1 is the level of the ground motions as scaled to the seismic design spectrum.

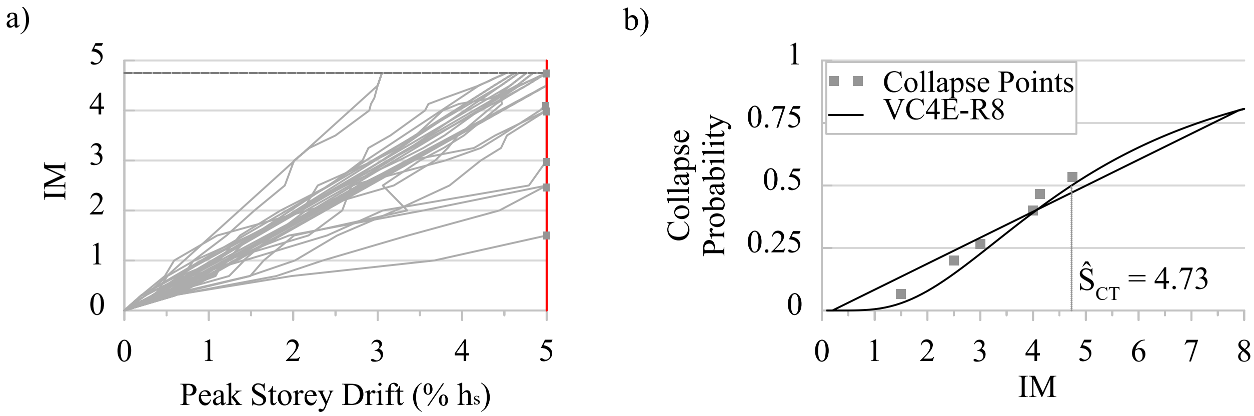

Figure 13 a) TIDA results; and b) Resulting fragility curve for Building VC4E-R8.

As required in the FEMA P695 methodology, additional uncertainties were considered when generating the fragility curves, using:

$$\beta_{TOT} = \sqrt{\beta_{RTR}^2 + \beta_{DR}^2 + \beta_{TD}^2 + \beta_{MDL}^2} \quad (8)$$

where β_{TOT} is the total collapse uncertainty and β_{DR} , β_{TD} , β_{MDL} are respectively the uncertainties related to the design requirements, the test data used to calibrate the numerical model used in the analyses, and the modelling assumptions used to build the numerical model. As a result, the dispersion of the fragility curves widens. The design method used in this study to determine the frame resistance to overturning is considered to be robust enough to prevent collapse mechanisms that are not explicitly modelled in the analysis (e.g., member buckling or yielding, connection failures, etc.). Therefore, the uncertainty related to the design requirements was assigned a "superior" rating with $\beta_{DR} = 0.1$ [25]. The accuracy of the test data and numerical model were both assigned a rating of "good", leading to i.e. $\beta_{TD} = \beta_{MDL} = 0.2$.

The estimated values of $\hat{\beta}_{RTR}$ and $\hat{S}_{CT}$ are given in Table 2, as well as the probability of collapse for the design amplitude, i.e. *IM* = 1. As shown, the values of $\hat{\beta}_{RTR}$ vary from 0.32 to 0.82, with an average value of 0.5. The larger values are obtained for the taller buildings. Since the ground motions used to perform the TIDA were scaled for the period range of each building, as required in [23], the collapse margin ratio (*CMR*) of the buildings against overturning is equal to the estimated median collapse intensity, $\hat{S}_{CT}$. The spectral shape factor, *SSF*, was set equal to 1.0 in the generation of the fragility curves, which means that conservative collapse estimates were obtained here. Figure 14 presents the collapse fragility curves obtained for some of the 22 buildings studied.

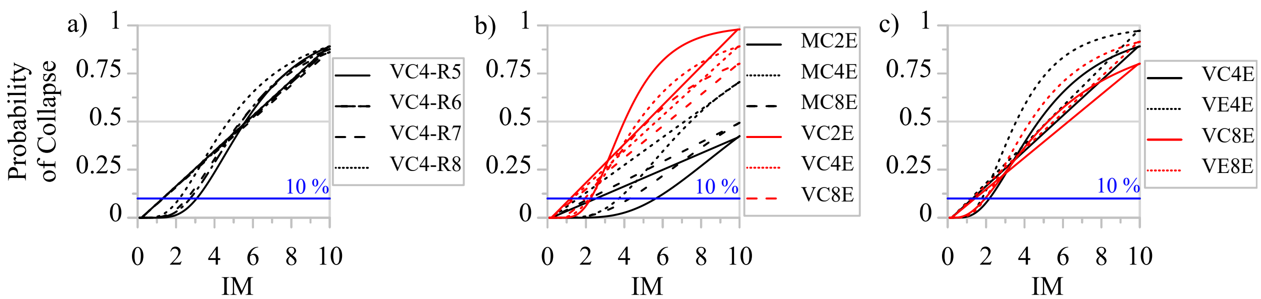

Figure 14 Collapse fragility curves: a) Influence of the R_{eff} factor; b) Influence of the seismicity and building height; and c) Influence of the site class.

As shown in Table 2, for all cases presented, *CMR* is higher than 3.6. In this study, rather than comparing the *CMR* with the acceptable value proposed in [25], it is read directly from the collapse fragility curve as the probability of collapse for the design amplitude, i.e. *IM* = 1, and it is considered to be acceptable when less than 10%. As shown in Table 2, for all buildings, the probability of collapse is lower than 1.6% for all buildings, with a mean value of 0.37%. The seismic performance of G-CRBFs against overturning of the base rocking joint is therefore deemed acceptable. In Figure 14, *CMR* decreases as R_{eff} is increased, as was expected because peak storey drifts increase when R_{eff} is increased. Likewise, *CMR* decreases as the building height is increased, and it is lower for buildings subjected to higher displacement demands i.e. site class E *vs.* site class C, and western Canada *vs.* eastern Canada.

7. Conclusions

A numerical study was performed to examine the seismic response of gravity-controlled rocking braced frames (G-CRBFs) including the dynamic vertical response of the gravity framing supported by the uplifting braced frame columns. The study was also conducted to assess the influence of the dynamic response of the gravity framing on the braced frame members forces and verify if gravity loads were sufficient to provide safety against collapse by overturning for this framing system. Complementary analyses were performed to evaluate the effects of the vertical component of ground motions on the G-CRBF member forces, and examine the possible beneficial effect of the inherent friction in bolted beam-to-column connections on the frame drifts and member forces. Twenty-two buildings located in two seismically active regions of Canada were designed using response spectrum analysis. Different building heights and site classes were considered to identify conditions for which the system would be more effective.

The following conclusions can be drawn from the study:

- All G-CRBF frames studied showed satisfactory seismic response, with peaks storey drifts being well within permissible values. Storey drifts predicted with the equation proposed by Zhang et al. for PT-CRBFs were found to be within 10% of the storey drifts obtained from NLRHA for the frames designed with $\beta \geq 0.4$.
- The dynamic response of the gravity framing system induced significant additional beam shear and moment demands that need to be considered in the design, due to the floor vibration modes.

- The design procedure used in this study gave an accurate estimation of the peak axial loads in the braced frame columns. Peak axial loads in the braces were underestimated by 14%, on average, by the design method. This difference is attributed to the additional inertia forces induced by the dynamic vertical response of the beams supported by the G-CRBFs.
- Including vertical masses corresponding to the vertical loads supported by G-CRBFs in the RSA used for design had a limited influence on member forces and this influence tends to diminish relative to that of the lateral higher modes for taller buildings. It is therefore not necessary to include these masses in design of mid-rise G-CRBFs. However, including these masses is recommended for low-rise buildings.
- The fragility curves developed in the study showed that all the G-CRBF buildings studied demonstrate acceptable margins against collapse by overturning of the rocking joint according to the FEMA P695 criteria.

The fragility curves examined in this study were developed with elastic frame models to investigate the risk of collapse by overturning. In future studies, fragility curves from analyses in which inelastic member response is explicitly modelled should be generated to assess the robustness of the G-CRBF system and the design procedure. Further studies on taller G-CRBF buildings should be performed to confirm the findings of this study. Results from such additional studies are necessary to complete the development of a proper design method for gravity-controlled rocking braced frame buildings.

8. Acknowledgments

Financial support for this research was provided by the Fonds de Recherche Nature et Technologies (FRQNT) of the Government of Quebec and the Natural Sciences and Engineering Research Council (NSERC) of Canada. The authors express their appreciation to Bashar Hariri, Ph.D.

Candidate at Polytechnique Montreal, for the selection and scaling of the ground motions used in this study.

9. References

[1] Midorikawa M, Azuhata T, Ishihara T, Wada A, (2006): Shaking table tests on seismic response of steel braced frames with column uplift. Earthquake Engineering and Structural Dynamics; 35:1767–1785.

[2] Sause R, Ricles JM, Roke DA, Chancellor NB, Gonner NP, (2010): Seismic performance of a self-centring rocking concentrically-braced frame. Proc. 9th US National and 10th Canadian Conference on Earthquake Engineering, Toronto, Canada, Paper No 1330.

[3] Wiebe L, Christopoulos C, Tremblay R, and Leclerc M, (2013): Mechanisms to limit higher mode effects in a controlled rocking steel frame. 1: Concept, modelling, and low-amplitude shake table testing. Earthquake Engineering and Structural Dynamics, 42 (7), 1053–1068.

[4] Deierlein G, Ma X, Eatherton MR, Hajjar J, Krawinkler H, Takeuchi T, Kasai K, Midorikawa M, (2011): Earthquake resilient steel braced frames with controlled rocking and energy dissipating fuses. Steel Construction, 4 (3): 171–175.

[5] Tremblay R, Poirier L-P, Bouaanani N, (2008): Innovative viscously damped rocking braced steel frames. Proc. 14th World Conference on Earthquake Engineering, Beijing, China, Paper No 05-01-0527.

[6] Mottier P, Tremblay R, Rogers C, (2018): Seismic Retrofit of Low-Rise Steel Buildings in Canada using Rocking Steel Braced Frames. Earthquake Engineering and Structural Dynamics, 47 (2), 333–355.

[7] Tremblay R, Mottier P, (2020): A simple self-centring shear fuse for cost-effective controlled rocking steel braced frames. Proc. 17th World Conference on Earthquake Engineering, Sendai, Japan. (submitted).

[8] Mottier P, Tremblay R, Rogers C, (2020): Shake-table test of a 2-storey steel building seismically retrofitted using gravity-controlled rocking braced frame system. Earthquake Engineering and Structural Dynamics (submitted).

[9] Mottier P, Tremblay R, Rogers CA, Wiebe L (2020): Influence of vertical masses on the response of gravity-controlled rocking braced frames. Proc. 17th World Conference on Earthquake Engineering, Sendai, Japan. (submitted).

[10] NRCC (2015): National Building Code of Canada 2015, 14th ed. National Research Council of Canada (NRCC), Ottawa, ON, Canada.

[11] Opensees, (2012): Open system for earthquake engineering simulation v3.0.3 [Computer Software]. https://opensees.berkeley.edu/

[12] Dyanati M, Huang Q, Roke D (2015): Seismic demand models and performance evaluation of self-centring and conventional concentrically braced frames. Engineering Structures, 84 (2), 368–381.

[13] Steele TC, Wiebe LDA (2017): Collapse risk of controlled rocking steel braced frames with different post-tensioning and energy dissipation designs. Earthquake Engineering and Structural Dynamics, 46 (13), 2063–2082. doi: 10.1002/eqe.2892.

[14] CSA (2019): CSA S16-19, Design of Steel Structures. Canadian Standards Association (CSA), Toronto, ON, Canada.

[15] AISC (2016): Vibrations of steel-framed structural systems due to human activity: AISC Design Guide 11, American Institute of Steel Construction.

[16] Earthquakes Canada, GSC, Continuous Waveform Archive, http://earthquakescanada.nrcan.gc.ca/stndon/AutoDRM/index-eng.php

[17] Christopoulos C, Filiatrault A, & Folz B (2002): Seismic response of self-centring hysteretic SDOF systems. Earthquake Engineering and Structural Dynamics, 31 (5), 1131-1150.

[18] Wiebe L, Christopoulos C. (2009): Mitigation of higher mode effects in base-rocking systems by using multiple rocking sections. Journal of Earthquake Engineering, 13(S1), 83-108.

[19] CSA (2014): CSA S6-14, Canadian Highway Bridge Design Code. Canadian Standards Association (CSA), Toronto, ON, Canada.

[20] Zhang C, Steele TC, Wiebe LD (2018): Design-level estimation of seismic displacements for self-centring SDOF systems on stiff soil. Engineering Structures, 177, 431–443.

[21] Mottier P (2020): Analyses numérique et expérimentale du comportement sismique des contreventements berçants gravitaires en acier. *Ph.D. Thesis*. Polytechnique Montreal *(in French).*

[22] Mottier P, Tremblay R, Rogers C (2019): Full-scale impact tests of columns for rocking steel braced frames. Proceedings of the 12th Canadian Conference on Earthquake Engineering, Quebec, Canada.

[23] NRCC (2017): Structural Commentaries (User's Guide — NBC 2015: Part 4 of Division B), 4th ed. National Research Council of Canada, Ottawa, ON.

[24] Atkinson, G M (2009): Earthquake time histories compatible with the 2005 National building code of Canada uniform hazard spectrum. Canadian Journal of Civil Engineering, 36 (6), 991-1000.

[25] Applied Technology Council (2009): Quantification of building seismic performance factors, FEMA Report P695, Federal Emergency Management Agency, Washington, DC, United States.

[26] Vamvatsikos D, Cornell CA (2002): Incremental dynamic analysis. Earthquake Engineering and Structural Dynamics, 31 (3), 491–514.

[27] Baker J (2015): Efficient analytical fragility function fitting using dynamic structural analysis. Earthquake Spectra; 31 (1), 579–599.